Geometric Tracking Control of Aerial Robots Based on Centroid Vectoring

Lovro Marković, Antun Ivanović, Marko Car, Matko Orsag, Stjepan Bogdan

Abstract— **This paper focuses on presenting the concept of geometric tracking control for an unmanned aerial vehicle (UAV) based on variations in center of gravity (CoG). The proposed UAV model has the ability to exploit its dynamic CoG as a means of stabilization and control. A mathematical model of such a system is used as a base for developing the nonlinear geometric tracking controller on the special Euclidean group SE(3). Finally, two unique UAV models, presented with a trajectory tracking problem, are simulated in a realistic simulation environment. Performance of the selected control terms is analyzed based on relevant simulation results.**

I. INTRODUCTION

Geometric control concept has previously been applied for classic quadrotor vehicles in [1], [2], [3] set up in plus configuration with their CoG located inside the origin of the UAV body frame. Since a unique type of UAV is considered in this paper its mathematical model differs from aforementioned research. Unlike a standard UAV, whose CoG coincides with its body-fixed frame origin, it utilizes variations in CoG in order to achieve attitude tracking and stability. Essentially, this means that such variations, which would usually be considered a disturbance in the system, could be exploited as a means of controlling the UAV. Since a geometric controller is used in this paper, model dynamics need to be expressed on the SE(3) configuration manifold. It is important to note that unlike traditional quadrotor dynamics, CoG vector $\mathbf{r}_{CoG}$ is also included in the mathematical model. One of the ways these variations are achieved is by implementing the moving mass control concept (MMC)[4] on the standard quadrotor UAV. This includes mounting moving masses on the UAV arms, which offset acts as the control input of the system along with rotor speed variation. This is a novel concept first developed in [5] with attitude control considered in [6]. Up to this point, nonlinear geometric control has not been applied to the moving-mass controlled UAV.

Furthermore, CoG variations are achieved by mounting two manipulators to the UAV, each carrying a payload. In this case position of the payload directly determines any difference in CoG. UAVs endowed with manipulators have previously been studied in [7], [8]. Similar problem has

already been presented in [9] where end-effector trajectory tracking of a single mounted manipulator is considered. However, in this paper, along with a different approach in controller synthesis and system modeling, two 2-DOF manipulators are used, each carrying a payload. The main subject for trajectory tracking is still the UAV, while manipulators are considered an extension, used only for attitude control.

Therefore, the goal of this paper is to present the appropriate dynamic model for UAVs with variable CoG on the SE(3) configuration manifold, choose control terms based on that model and evaluate controller performance on a predefined trajectory tracking problem using two unique UAV models described previously.

For realistic Gazebo simulations, we use μMORUS UAV, which is a scaled down version of the UAV developed within the MORUS project [10].

The paper is organized as follows. First the general mathematical model is presented on the SE(3) configuration manifold along with expressions for CoG and moments of inertia. Using that mathematical model, control terms are chosen such that desirable error dynamics can be obtained. Sufficient stability conditions are presented for the obtained error dynamics. Lastly, two sets of simulations are conducted using the Gazebo simulator and ROS environment. Both UAVs are compared using the same trajectory tracking problem in order to assess performance of each approach.

II. MATHEMATICAL MODEL

First of all, it is necessary to introduce a fixed inertial reference frame $\{\mathbf{e}_1, \mathbf{e}_2, \mathbf{e}_3\}$ and a body-fixed frame $\{\mathbf{b}_1, \mathbf{b}_2, \mathbf{b}_3\}$. Next, we present a general equation for calculating CoG vector from the origin of the body-fixed frame as follows:

$$\mathbf{r}_{CoG} = \frac{m_b\mathbf{r}_b + \sum_{i=1}^{n} m_i\mathbf{r}_i}{m_b + \sum_{i=1}^{n} m_i} = \frac{\sum_{i=1}^{n} m_i\mathbf{r}_i}{m_t}, \quad (1)$$

The following terms are defined as:

- $\mathbf{r}_{CoG} \in \mathrm{R}^3$ - CoG with respect to the body-fixed frame
- $\mathbf{r}_i \in \mathrm{R}^3$ - Position of the i-th mass or payload w.r.t. the body-fixed frame
- $\mathbf{r}_b \in \mathrm{R}^3$ - Position of UAV body w.r.t. the body-fixed frame. Note that because the body frame origin coincides with the rigid body CoG (without

Authors are with Faculty of Electrical and Computer Engineering, University of Zagreb, 10000 Zagreb, Croatia (Antun Ivanović, Marko Car, Tomislav Haus, Matko Orsag, Stjepan Bogdan, Lovro Marković) at fer.hr

considering the moving masses) this term yields $\mathbf{r}_b = 0_{3x1}$

- $m_b \in \mathbb{R}$ - Mass of the UAV body
- $m_i \in \mathbb{R}$ - Mass of the i-th moving mass or payload
- $m_t \in \mathbb{R}$ - Mass of the whole UAV system

Moment of inertia matrix expressed in the body-fixed frame is defined as follows:

$$\mathrm{J} = \mathrm{J}_b + \sum_{i=1}^{n} \mathrm{J}_i, \tag{2}$$

where $\mathrm{J}_b \in \mathbb{R}^3$ is body and $\mathrm{J}_i \in \mathbb{R}^3$ is the moment of inertia of some mass element outside the origin of the body-fixed frame. Using the parallel axis theorem, one is able to calculate J_i while knowing the moment of inertia around its CoG:

$$\mathrm{J}_i = \mathrm{J}_{i,CoG} + m_i(\mathbf{r}_i^T \cdot \mathbf{r}_i \mathrm{I}_{3\times3} - \mathbf{r}_i \cdot \mathbf{r}_i^T) \tag{3}$$

Now we can express the equations of motion in the inertial frame while taking in consideration CoG vector which is located outside the origin of the body-fixed frame[11].

The complete model dynamics expressed in the inertial frame are presented and derived in V. It is important to note that the terms containing changes of the moment of inertia and CoG have been omitted from (50) and (51). The proposed model is presented as follows:

$$m_t\ddot{\mathbf{x}} - m_t\mathrm{R}(\mathbf{r}_{CoG} \times \dot{\boldsymbol{\Omega}}) + m_t g\mathbf{e}_3 = f\mathrm{R}\mathbf{e}_3 \tag{4}$$

$$\dot{\mathrm{R}} = \mathrm{R}\hat{\boldsymbol{\Omega}} \tag{5}$$

$$\begin{aligned} \mathrm{J}\dot{\boldsymbol{\Omega}} + m_t\mathbf{r}_{CoG} \times \mathrm{R}^T\ddot{\mathbf{x}} + \boldsymbol{\Omega} \times \mathrm{J}\boldsymbol{\Omega} \\ - m_t(\boldsymbol{\Omega} \times \mathbf{r}_{CoG}) \times \mathrm{R}^T\dot{\mathbf{x}} = \mathbf{M} \end{aligned} \tag{6}$$

The *hat map* is an operator equivalent to the expression $\hat{\mathbf{x}}\mathbf{y} = \mathbf{x} \times \mathbf{y}$. It maps elements of $\mathbb{R}^3$ to the so(3) Lie algebra.

The following terms are defined as:

- $\mathrm{J} \in \mathbb{R}^{3\times3}$ - Moment of inertia matrix w.r.t. the body-fixed frame
- $\mathrm{R} \in SO(3)$ - Rotation matrix from the body fixed frame to the inertial frame
- $\boldsymbol{\Omega} \in \mathbb{R}^3$ - Angular velocity in the body-fixed frame
- $\mathbf{x} \in \mathbb{R}^3$ - Location of the body-fixed frame in the inertial frame
- $\mathbf{v} \in \mathbb{R}^3$ - Velocity of the body-fixed frame in the inertial frame
- $f \in \mathbb{R}$ - Total thrust produced by the UAV
- $\mathbf{M} \in \mathbb{R}^3$ - Total moments acting in the body-fixed frame

Equations (4), (5) and (6) describe the dynamical flow of a rotating and translating rigid body in terms of evolution of $(\mathrm{R}, \mathbf{x}, \boldsymbol{\Omega}, \dot{\mathbf{x}}) \in \mathrm{TSE}(3)$ on the tangent bundle of SE(3).

Height and yaw of the UAV is controlled with variations in rotor velocity, whereas roll and pitch with variations in CoG. It is assumed that the first and the third propeller
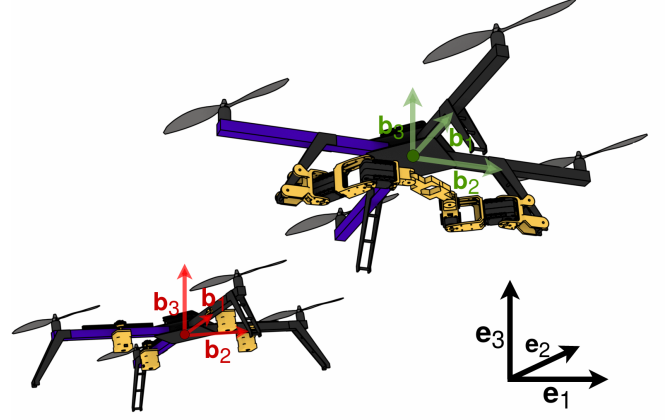

Fig. 1: UAV model with MMC (left) and two 2-DOF overactuated manipulators (right) along with their respective coordinate systems. The manipulator end effectors are placed diametrically opposite from each other.

rotate clockwise, while the second and the fourth rotate counter-clockwise. The relation between moments, thrust and rotor velocity is the following:

$$f_i = b_f\omega_i^2 \tag{7}$$

$$\tau_i = (-1)^i b_m f_i, \tag{8}$$

where the following terms are defined as:

- $f_i \in \mathbb{R}$ - Thrust of the i-th motor
- $\tau_i \in \mathbb{R}$ - Moment i-th motor produces
- $b_f \in \mathbb{R}$ - Motor thrust constant
- $b_m \in \mathbb{R}$ - Motor moment constant
- $\omega_i \in \mathbb{R}$ - Rotation velocity of the i-th rotor

Total thrust can be expressed as:

$$f = \sum_{1}^{4} f_i, \tag{9}$$

and total moment acting in the body-fixed frame as:

$$\begin{aligned} \mathbf{M} = [&m_p g d_x \mathbf{e}_1 \cdot \mathbf{b}_{3,d}, \\ &m_p g d_y \mathbf{e}_2 \cdot \mathbf{b}_{3,d}, \\ &b_m(-f_1 + f_2 - f_3 + f_4)], \end{aligned} \tag{10}$$

where $d_x \in \mathbb{R}$ and $d_y \in \mathbb{R}$ are moving mass or payload offsets along x and y axis respectively.

Using (9) and (10) as control inputs of the system one is able to obtain the desired force of each rotor and the control offsets d_x and d_y. While the control offsets are able to be directly applied as moving mass control inputs, in the manipulator case an additional transformation needs to take place.

Both manipulators are overactuated, meaning they have three actuators while operating in a 2-DOF workspace. They are placed in a diametrically opposite configuration as seen in 1, therefore only a single set of infinitesimal angle increments $\Delta q_1, \Delta q_2, \Delta q_3$ is sufficient as control input for both manipulators.

Conversion from payload offsets to angle increments is done using the inverse Jacobian of the manipulator end effector. Direct Jacobian matrix is presented as follows:

$$\begin{bmatrix} d_x \\ d_y \end{bmatrix} = \mathcal{J}(q_1, q_2, q_3) \cdot \begin{bmatrix} \Delta q_1 \\ \Delta q_2 \\ \Delta q_3 \end{bmatrix} \tag{11}$$

$$\mathcal{J} = \begin{bmatrix} l_1\cos(q_1) & l_2\cos(q_1 + q_2) & l_3\cos(q_1 + q_2 + q_3) \\ l_1\sin(q_1) & l_2\sin(q_1 + q_2) & l_3\sin(q_1 + q_2 + q_3) \end{bmatrix}, \tag{12}$$

where l_1, l_2 and l_3 are the manipulator link lengths, while q_1, q_2 and q_3 are current actuator angles. Using Jacobian pseudoinverse, incremental update rule for actuator angles can be obtained as follows:

$$\begin{bmatrix} \Delta q_1 \\ \Delta q_2 \\ \Delta q_3 \end{bmatrix} = \mathcal{J}^{-1}(q_1, q_2, q_3) \cdot \begin{bmatrix} d_x \\ d_y \end{bmatrix} \tag{13}$$

Manipulator and moving mass actuator dynamics along with the change in desired rotor force is regarded as instantaneous while presenting the controller synthesis and stability conditions. However, within the Gazebo simulation environment, a certain transfer dynamic is taken into account.

III. Geometric control on SE(3)

The main focus of the proposed controller is put on position tracking. Therefore, the trajectory consists of a desired position $\mathbf{x}_d(t)$ and a desired heading $\mathbf{b}_{1,d}(t)$ of the body-fixed frame. Since the given position is known ahead of time, one is able to calculate both desired linear velocity $\mathbf{v}_d(t)$ and acceleration $\mathbf{a}_d(t)$ which are also inherently included as inputs.

The controller is developed on the nonlinear Lie group SE(3) consisting of the rotation group SO(3) and translation group T(3). It is cascade in structure, as seen in 2 with position tracking block following attitude tracking block. The main advantage of using the SO(3) rotation group is to avoid any singularities or ambiguities that may arise when representing rotations with Euler angles or quaternions.

Controller synthesis is carried out as follows. First, position and orientation tracking errors are presented as the proportional and derivative part of the controller. In addition, nonlinear control terms are chosen to compensate proposed model dynamics. Finally, exponential stability conditions for the initial UAV configuration are shown.

A. Tracking errors

Compatible attitude error function and transport map between tangent bundles of SO(3) are chosen as suggested in [12] and confirmed in research regarding geometric control with aerial vehicles [3], [13], [2], [1]. Attitude error
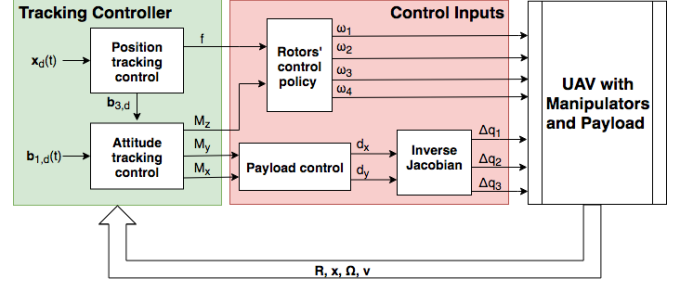

Fig. 2: Control scheme for the UAV carrying a payload. When considering UAV with MMC *Inverse Jacobian* block becomes the identity matrix. This means that the control inputs d_x and d_y are directly sent as system inputs.

function on SO(3) $\Psi(\mathrm{R}, \mathrm{R}_d)$ along with its compatible transport map $\mathcal{T}(\mathrm{R}, \mathrm{R}_d)$ are chosen as:

$$\Psi(\mathrm{R}, \mathrm{R}_d) = \frac{1}{2}tr[I - \mathrm{R}_d^T\mathrm{R}] \tag{14}$$

$$\mathcal{T}(\mathrm{R}, \mathrm{R}_d) = \mathrm{R}^T\mathrm{R}_d \tag{15}$$

Linear position and velocity tracking errors are defined as follows:

$$\mathbf{e}_x = \mathbf{x} - \mathbf{x}_d \tag{16}$$

$$\mathbf{e}_v = \mathbf{v} - \mathbf{v}_d \tag{17}$$

It is shown in [12] that the attitude tracking error should be chosen as a left-differential of the attitude error function $\Psi(\mathrm{R}, \mathrm{R}_d)$ as follows:

$$\mathbf{e}_\mathrm{R} = \frac{1}{2}(\mathrm{R}_d^T\mathrm{R} - \mathrm{R}^T\mathrm{R}_d)^{\mathrm{V}} \tag{18}$$

Due to the fact that angular velocities $\mathbf{\Omega} \in T_\mathrm{R}SO(3)$ and $\mathbf{\Omega}_d \in T_{\mathrm{R}_d}SO(3)$ evolve in different tangential bundles, the proposed left transport map (15) needs to be applied when calculating the angular velocity tracking error:

$$\mathbf{e}_\Omega = \mathbf{\Omega} - \mathrm{R}^T\mathrm{R}_d\mathbf{\Omega}_d \tag{19}$$

B. Control terms

After defining all tracking errors, one can start constructing the control terms. Taking in consideration the proposed system dynamics (4) and (6), the force and moment control terms are chosen as follows:

$$\begin{aligned} \mathbf{A} =&(-\mathrm{k}_x\mathbf{e}_x - \mathrm{k}_v\mathbf{e}_v + m\ddot{\mathbf{x}}_d \\ &+ mg\mathbf{e}_3 - m_t\mathrm{R}(\mathbf{r}_{CoG} \times \dot{\mathbf{\Omega}}) \\ f =&\mathbf{A} \cdot \mathrm{R}\mathbf{e}_3 \end{aligned} \tag{20}$$

$$\begin{aligned} \mathbf{M} =& -\mathrm{k}_\mathrm{R}\mathbf{e}_\mathrm{R} - \mathrm{k}_\Omega\mathbf{e}_\Omega \\ & -\mathrm{J}(\hat{\mathbf{\Omega}}\mathrm{R}^T\mathrm{R}_d\mathbf{\Omega}_d - \mathrm{R}^T\mathrm{R}_d\dot{\mathbf{\Omega}}_d) \\ & +\mathbf{\Omega} \times \mathrm{J}\mathbf{\Omega} + m\mathbf{r}_{CoG} \times \mathrm{R}^T\ddot{\mathbf{x}} \\ & -m(\mathbf{\Omega} \times \mathbf{r}_{CoG}) \times \mathrm{R}^T\dot{\mathbf{x}} \end{aligned} \tag{21}$$

Desired rotation matrix is constructed in the conventional way when considering geometric control of aerial

vehicles [1], [2], [13]. The proposed desired rotation matrix is constructed as $R_d = [\mathbf{b}_{1,c}, \mathbf{b}_{3,d} \times \mathbf{b}_{1,c}, \mathbf{b}_{3,d}]$ where component vectors of R_d are calculated in the following way:

$$\mathbf{b}_{3,d} = \frac{\mathbf{A}}{||\mathbf{A}||} \tag{22}$$

$$\mathbf{b}_{1,c} = -\frac{(\mathbf{b}_{3,d} \times (\mathbf{b}_{3,d} \times \mathbf{b}_{1,d}))}{||\mathbf{b}_{3,d} \times \mathbf{b}_{1,d}||} \tag{23}$$

The chosen constraint for the trajectory tracking problem differ slightly from the one proposed in [1]. Due to the fact that model dynamics which include variable CoG are considered in this paper, new trajectory constraints are presented as follows:

$$||mge_3 + m\ddot{\mathbf{x}}_d - mR\mathbf{r}_{CoG} \times \dot{\boldsymbol{\Omega}} - mR\hat{\boldsymbol{\Omega}}\hat{\mathbf{r}}_{CoG}\boldsymbol{\Omega}|| < B, \tag{24}$$

where B is some positive constant.

Desired angular velocity and acceleration also need to be considered in this trajectory tracking problem. One is able to calculate the desired angular velocity and acceleration using R_d and its derivatives in the following way:

$$\hat{\boldsymbol{\Omega}}_d = R_d^T \dot{R}_d \tag{25}$$

$$\dot{\hat{\boldsymbol{\Omega}}}_d = -\hat{\boldsymbol{\Omega}}_d \hat{\boldsymbol{\Omega}}_d + R_d^T \ddot{R}_d \tag{26}$$

Derivatives of R_d are calculated using the backwards differentiation method. Another important note is that the computation rate of the desired angular velocity and acceleration is slower than the overall simulation rate. For further implementation details, please refer to [14].

C. Error dynamics

In order to express error dynamics, one needs to calculate the time derivatives of linear (17) and angular (19) tracking errors:

$$\mathbf{e}_v = \dot{\mathbf{x}} - \dot{\mathbf{x}}_d \tag{27}$$

$$\mathbf{e}_\Omega = \dot{\boldsymbol{\Omega}} + \hat{\boldsymbol{\Omega}}R^T R_d \boldsymbol{\Omega}_d - R^T R_d \dot{\boldsymbol{\Omega}}_d \tag{28}$$

After including (4) and (6) in (27) and (28) respectively, the following equations are obtained:

$$\begin{aligned} m\mathbf{e}_v = & -mg\mathbf{e}_3 - m\ddot{\mathbf{x}}_d \\ & + m_t R(\mathbf{r}_{CoG} \times \dot{\boldsymbol{\Omega}}) \\ & + \mathbf{A} + \mathbf{X} \end{aligned} \tag{29}$$

$$\begin{aligned} J\mathbf{e}_\Omega = & J(\hat{\boldsymbol{\Omega}}R^T R_d \boldsymbol{\Omega}_d - R^T R_d \dot{\boldsymbol{\Omega}}_d) \\ & - \boldsymbol{\Omega} \times J\boldsymbol{\Omega} + m_t \mathbf{r}_{CoG} \times R^T \ddot{\mathbf{x}} \\ & + m_t(\boldsymbol{\Omega} \times \mathbf{r}_{CoG}) \times R^T \dot{\mathbf{x}} \\ & + \mathbf{M} \end{aligned} \tag{30}$$

Note that in (29) $\mathbf{X} \in R^3$ is a bounded term which equals:

$$\mathbf{X} = \frac{f}{(R_d\mathbf{e}_3)^T R\mathbf{e}_3}(R_d\mathbf{e}_3 - ((R_d\mathbf{e}_3)^T R\mathbf{e}_3)R\mathbf{e}_3) \tag{31}$$

After substituting control force from (20) and (21) in (29) and (30) respectively the final form of error dynamics is obtained:

$$m\mathbf{e}_v = -k_x\mathbf{e}_x - k_v\mathbf{e}_v + \mathbf{X} \tag{32}$$

$$J\mathbf{e}_\Omega = -k_R\mathbf{e}_R - k_\Omega\mathbf{e}_\Omega \tag{33}$$

D. Stability discussion

We begin by observing (32) and (33). It has to be taken in account that the derived error dynamics are identical to those presented in [3] and [1], even though the proposed model and control terms in this paper differ from previous research.

Therefore, to avoid redundancy, the complete stability proof is omitted for brevity. Instead, only final conclusions for attitude error function $\Psi(R(t), R_d(t))$ exponential asymptotic stability and tracking error attraction to the zero-equilibrium state are outlined as established in [3].

Granted the initial UAV configuration satisfies the following conditions:

$$\Psi(R(0), R_d(0)) < 2 \tag{34}$$

$$||\mathbf{e}_\Omega(0)||^2 < \frac{2}{\lambda_{min}(J)}k_R(2 - \Psi(R(0), R_d(0))), \tag{35}$$

it can be shown that tracking errors of the whole system reaches zero-equilibrium state and the attitude function is exponentially bounded as:

$$\Psi(R(t), R_d(t)) \leq \min\{2, \alpha e^{-\beta t}\} \tag{36}$$

for some positive constants α and β.

IV. SIMULATION

Simulations are conducted in the Gazebo simulator within the ROS environment. UAV used in experiments is the μMorus which can be found in the *mmuav_gazebo* repository [14], along with its model parameters. Two experiments are conducted with UAVs using two different methods of CoG variation: MMC in the first case and payload carried by manipulators in the second case. Control parameters for the first case are chosen as follows:

$$k_x = \begin{bmatrix} 10 & 0 & 0 \\ 0 & 10 & 0 \\ 0 & 0 & 50 \end{bmatrix}, k_v = \begin{bmatrix} 3.75 & 0 & 0 \\ 0 & 3.75 & 0 \\ 0 & 0 & 20 \end{bmatrix},$$

$$k_R = \begin{bmatrix} 1.5 & 0 & 0 \\ 0 & 1.5 & 0 \\ 0 & 0 & 10 \end{bmatrix}, k_\Omega = \begin{bmatrix} 0.65 & 0 & 0 \\ 0 & 0.65 & 0 \\ 0 & 0 & 1.54 \end{bmatrix},$$

Rotational control parameters, in the second case, stay the same, while translational parameters are the following:

$$k_x = \begin{bmatrix} 7.2 & 0 & 0 \\ 0 & 7.2 & 0 \\ 0 & 0 & 50 \end{bmatrix}, k_v = \begin{bmatrix} 2.6 & 0 & 0 \\ 0 & 2.6 & 0 \\ 0 & 0 & 20 \end{bmatrix},$$

For both cases, initial parameters are obtained by considering the error dynamics (32) and (33) in the equilibrium state. However, they are further tuned with better position tracking performance in mind.

It is important to note that the actuator dynamics of moving masses and manipulators is taken in consideration within the Gazebo simulator. Furthermore there is a slight transient delay while increasing or decreasing rotor velocity which results in a non-instantaneous control force change.

The chosen trajectory tracking problem is formulated as a rotating spiral:

$$\mathbf{x}_d(t) = [0.4t; \; 0.5\sin(\pi t); \; 0.6\cos(\pi t) + 2]$$
$$\mathbf{b}_{1,d}(t) = \left[\cos\left(\frac{\pi}{5}t\right); \; \sin\left(\frac{\pi}{5}t\right); \; 0\right]$$
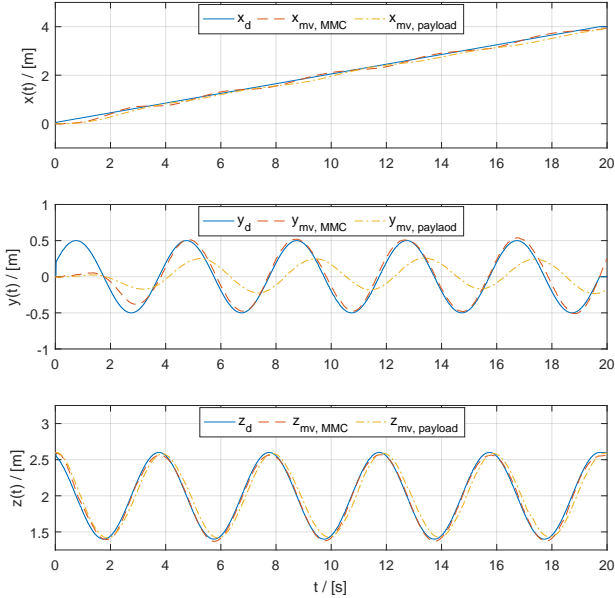

Fig. 3: Comparison between desired $\mathbf{x}_d$ and measured position values $\mathbf{x}_{mv}$ for both simulation cases. While tracking on x and z axes are reasonably similar, slower position tracking can be observed on the y axis for the second simulation case. Calculated MSE values are 0.0079 and 0.00352 for first and second case respectively.

V. Conclusion

Geometric control was presented and implemented for two separate UAV models with variable centers of gravity. Although the controller has been constructed without actuator dynamics in mind, during the simulations its effect can be seen.

Moving mass actuator dynamics have a noticeably faster transient effect than the manipulator dynamics. This claim can be affirmed by observing 6 where variations in CoG produced by MMC occur quicker and achieve
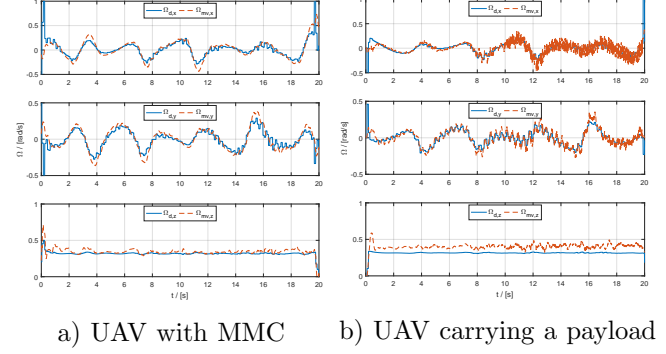

a) UAV with MMC   b) UAV carrying a payload

Fig. 4: Comparison between desired $\mathbf{\Omega}_d$ and measured $\mathbf{\Omega}_{mv}$ angular velocities for both simulation cases. Better angular velocity tracking is achieved in the first case, while in the second case an oscillatory measured value is observed around x axis during later stages of trajectory tracking. It is interesting to note that although desired position and heading are the same for each case, a different desired angular velocity is obtained using (25).
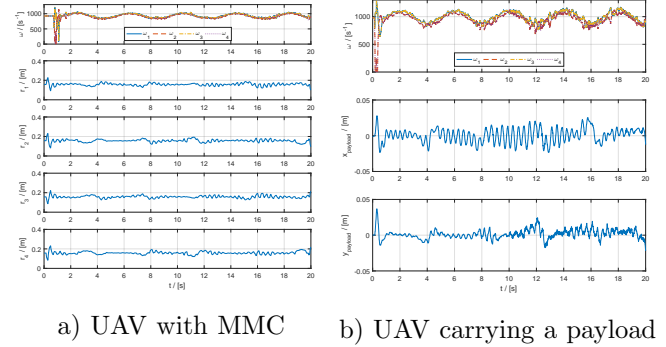

a) UAV with MMC   b) UAV carrying a payload

Fig. 5: Figures show control inputs for both simulation cases: rotor velocities ω_i, moving mass and payload offsets r_i. Rotor velocities are similar because desired trajectory height is equal for both cases.

greater magnitudes than those produced by the carried payload. Therefore, it is expected that the UAV with MMC achieves better position and attitude tracking than UAV carrying a payload. In 3 it can be seen that this expectation is validated. In the first case(MMC) excellent tracking performance can be observed, while in the second case(payload) measured position along the y-axis exhibits tracking delay and lower magnitude with respect to the desired position.

The overall effect of control terms 20 and 21 which include $\mathbf{r}_{CoG}$ becomes negligible if considering slower trajectories. In such cases, both UAVs can be observed as having CoG inside the origin of the body-fixed frame yielding simpler control terms.

APPENDIX

In this section rotating body dynamics with variations in center of gravity is derived. General form of Euler-
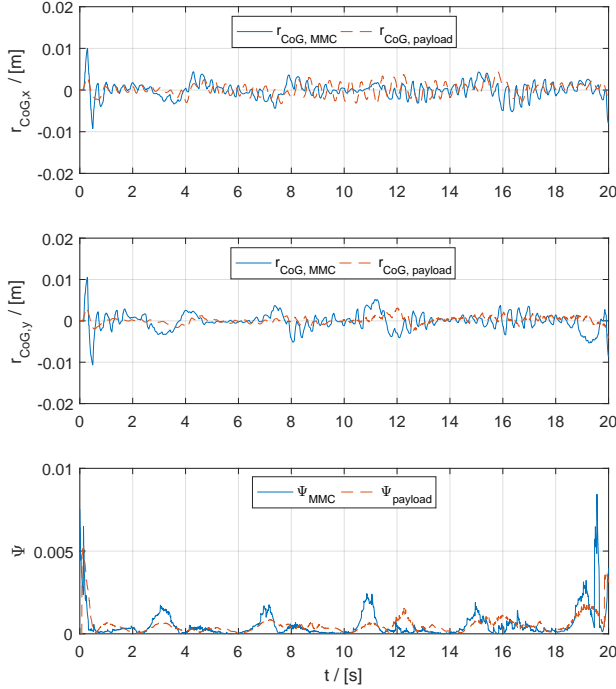
Fig. 6: Comparison between first two components of CoG vector $\mathbf{r}_{CoG}$ and between attitude error functions Ψ for both simulation cases. It can be seen that higher magnitude of CoG variation can be achieved using moving masses rather than the carried payload.

Lagrange dynamics for a rotating rigid body in SE(3) configuration manifold in the body-fixed frame as presented in [11]:

$$\frac{d}{dt}\left(\frac{\partial \mathcal{L}}{\partial \boldsymbol{\Omega}}\right) + \boldsymbol{\Omega} \times \frac{\partial \mathcal{L}}{\partial \boldsymbol{\Omega}} + \mathbf{v} \times \frac{\partial \mathcal{L}}{\partial \mathbf{v}} + \sum_{i=1}^{3}\mathbf{r}_i \times \frac{\partial \mathcal{L}}{\partial \mathbf{r}_i} = 0 \tag{37}$$

$$\frac{d}{dt}\left(\frac{\partial \mathcal{L}}{\partial \mathbf{v}}\right) + \boldsymbol{\Omega} \times \frac{\partial \mathcal{L}}{\partial \mathbf{v}} - \mathrm{R}^T \frac{\partial \mathcal{L}}{\partial x} = 0 \tag{38}$$

For the the proposed UAV with variations in CoG the Lagrangian is:

$$\mathcal{L}(\mathrm{R}, x, \boldsymbol{\Omega}, \mathbf{v}) = \frac{1}{2}\boldsymbol{\Omega}^T \mathrm{J}\boldsymbol{\Omega} + m\boldsymbol{\Omega}^T \hat{\mathbf{r}}_{CoG}\mathbf{v} + \frac{1}{2}m\mathbf{v}^T\mathbf{v} - U(\mathrm{R}, \mathbf{x}), \tag{39}$$

where $U(\mathrm{R}, \mathbf{x})$ is the potential energy of the system. It is important to note that J and $\mathbf{r}_{CoG}$ are variable over time.

Lagrangian derivatives needed for the general form equations 37 and 38 are:

$$\frac{\partial \mathcal{L}}{\partial \boldsymbol{\Omega}} = \mathrm{J}\boldsymbol{\Omega} + m\hat{\mathbf{r}}_{CoG}\mathbf{v} \tag{40}$$

$$\frac{d}{dt}\left(\frac{\partial \mathcal{L}}{\partial \boldsymbol{\Omega}}\right) = \dot{\mathrm{J}}\boldsymbol{\Omega} + \mathrm{J}\dot{\boldsymbol{\Omega}} + m\dot{\mathbf{r}}_{CoG} \times \mathbf{v} + m\mathbf{r}_{CoG} \times \dot{\mathbf{v}} \tag{41}$$

$$\frac{\partial \mathcal{L}}{\partial \mathbf{v}} = m\mathbf{v} - m\mathbf{r}_{CoG} \times \boldsymbol{\Omega} \tag{42}$$

$$\frac{d}{dt}\left(\frac{\partial \mathcal{L}}{\partial \mathbf{v}}\right) = m\dot{\mathbf{v}} - m\dot{\mathbf{r}}_{CoG} \times \boldsymbol{\Omega} - m\mathbf{r}_{CoG} \times \dot{\boldsymbol{\Omega}} \tag{43}$$

It is of interest to transfer rotation and translation dynamics in the inertial frame. This can be done using the following relations:

$$\mathbf{v} = \mathrm{R}^T \dot{x} \tag{44}$$
$$\dot{\mathbf{v}} = \mathrm{R}^T \ddot{\mathbf{x}} - \boldsymbol{\Omega} \times (\mathrm{R}^T \dot{\mathbf{x}}) \tag{45}$$
$$\mathbf{r}_{CoG} = \mathrm{R}^T (\mathbf{x}_{CoG} - \mathbf{x}) \tag{46}$$
$$\dot{\mathbf{r}}_{CoG} = \mathrm{R}^T(\dot{\mathbf{x}}_{CoG} - \dot{\mathbf{x}}) - \hat{\boldsymbol{\Omega}}\mathrm{R}^T(\mathbf{x}_{CoG} - \mathbf{x}) \tag{47}$$

After plugging in 40, 41, 42, 43 in 37, 38 and using 44, 45 as transformations of velocity and acceleration to inertial frame the following equations are obtained:

$$\mathrm{J}\dot{\boldsymbol{\Omega}} + m\mathbf{r}_{CoG} \times \mathrm{R}^T\ddot{\mathbf{x}} + \boldsymbol{\Omega} \times \mathrm{J}\boldsymbol{\Omega}$$
$$+ \dot{\mathrm{J}}\boldsymbol{\Omega} + m\dot{\mathbf{r}}_{CoG} \times \mathrm{R}^T\dot{\mathbf{x}} + \sum_{i=1}^{3}\mathbf{r}_i \times \frac{\partial \mathcal{L}}{\partial \mathbf{r}_i} = 0 \tag{48}$$

$$m\ddot{\mathbf{x}} - m\mathrm{R}(\mathbf{r}_{CoG} \times \dot{\boldsymbol{\Omega}}) - m\mathrm{R}(\dot{\mathbf{r}}_{CoG} \times \dot{\boldsymbol{\Omega}})$$
$$- m\mathrm{R}[\boldsymbol{\Omega} \times (\mathbf{r}_{CoG} \times \boldsymbol{\Omega})] + \frac{\partial U(\mathrm{R}, \mathbf{x})}{\partial \mathbf{x}} = 0 \tag{49}$$

Finally, CoG transform 46, 47 is included along with forces and moments acting in the body-fixed frame and potential energy of the system which gives the following model dynamics:

$$\mathrm{J}\dot{\boldsymbol{\Omega}} + m\mathbf{r}_{CoG} \times \mathrm{R}^T\ddot{\mathbf{x}} + \boldsymbol{\Omega} \times \mathrm{J}\boldsymbol{\Omega}$$
$$- m(\boldsymbol{\Omega} \times \mathbf{r}_{CoG}) \times \mathrm{R}^T\dot{\mathbf{x}} \tag{50}$$
$$+ \dot{\mathrm{J}}\boldsymbol{\Omega} + m\widehat{R^T(\dot{\mathbf{x}}_{CoG} - \dot{\mathbf{x}})}R^T\dot{\mathbf{x}} = \mathbf{M}$$

$$m\ddot{\mathbf{x}} - m\mathrm{R}(\mathbf{r}_{CoG} \times \dot{\boldsymbol{\Omega}}) + mg\mathbf{e}_3$$
$$- m\mathrm{R}\widehat{R^T(\dot{\mathbf{x}}_{CoG} - \dot{\mathbf{x}})}\boldsymbol{\Omega} = f\mathrm{R}\mathbf{e}_3 \tag{51}$$

ACKNOWLEDGMENT

REFERENCES

[1] T. Lee, M. Leok, and N. H. McClamroch, "Geometric tracking control of a quadrotor uav on se(3)," in *49th IEEE Conference on Decision and Control (CDC)*, pp. 5420–5425, Dec 2010.

[2] T. Lee, M. Leok, and N. Harris McClamroch, "Nonlinear Robust Tracking Control of a Quadrotor UAV on SE(3)," *ArXiv e-prints*, Sept. 2011.

[3] T. Lee, M. Leok, and N. Harris McClamroch, "Control of Complex Maneuvers for a Quadrotor UAV using Geometric Methods on SE(3)," *ArXiv e-prints*, Mar. 2010.

[4] T. Haus, M. Orsag, and S. Bogdan, "Design considerations for a large quadrotor with moving mass control," in *2016 International Conference on Unmanned Aircraft Systems (ICUAS)*, pp. 1327–1334, June 2016.

[5] T. Haus, M. Orsag, and S. Bogdan, "Mathematical modelling and control of an unmanned aerial vehicle with moving mass control concept," *Journal of Intelligent & Robotic Systems*, vol. 88, pp. 219–246, Dec 2017.

[6] T. Haus, N. Prkut, K. Borovina, B. Marić, M. Orsag, and S. Bogdan, "A novel concept of attitude control for large multirotor-uavs based on moving mass control," in *2016 24th Mediterranean Conference on Control and Automation (MED)*, pp. 832–839, June 2016.

[7] M. Orsag, C. Korpela, S. Bogdan, and P. Oh, "Dexterous aerial robots—mobile manipulation using unmanned aerial systems," *IEEE Transactions on Robotics*, vol. 33, pp. 1453–1466, Dec 2017.

[8] C. Korpela, M. Orsag, M. Pekala, and P. Oh, "Dynamic stability of a mobile manipulating unmanned aerial vehicle," in *2013 IEEE International Conference on Robotics and Automation*, pp. 4922–4927, May 2013.

[9] H. Yang and D. Lee, "Dynamics and control of quadrotor with robotic manipulator," in *2014 IEEE International Conference on Robotics and Automation (ICRA)*, pp. 5544–5549, May 2014.

[10] "Morus project." `http://www.fer.unizg.hr/morus`. Accessed: 2017-09-08.

[11] T. Lee, M. Leok, and N. H. McClamroch, *Global formulations of Lagrangian and Hamiltonian dynamics on manifolds : a geometric approach to modeling and analysis*. Interaction of mechanics and mathematics series, Springer, 2018.

[12] A. D. L. Francesco Bullo, *Geometric control of mechanical systems: modeling, analysis, and design for simple mechanical control systems*. Texts in applied mathematics 49, Springer, 1 ed., 2005.

[13] T. Fernando, J. Chandiramani, T. Lee, and H. Gutierrez, "Robust adaptive geometric tracking controls on so(3) with an application to the attitude dynamics of a quadrotor uav," in *2011 50th IEEE Conference on Decision and Control and European Control Conference*, pp. 7380–7385, Dec 2011.

[14] "mmuav gazebo." `https://github.com/larics/mmuav_gazebo/tree/geometry_control`, 2018.

[15] A. D. L. Francesco Bullo, *Geometric control of mechanical systems: modeling, analysis, and design for simple mechanical control systems*. Texts in applied mathematics 49, Springer, 1 ed., 2005.

[16] F. P. Schuller, *Lectures on the Geometric Anatomy of Theoretical Physics*. Friedrich-Alexander-Universität Erlangen-Nürnberg, Institut für Theoretische Physik III, 2017.